# Optical properties of $Mo_6S_3I_6$ nanowires

D. Vengust,[1] F. Pfuner,[2] L. Degiorgi,[2] I. Vilfan,[1] V. Nicolosi,[3] J. N. Coleman,[3] and D. Mihailovic[1]
[1]*Complex Matter Department, Jozef Stefan Institute, Jamova 39, Ljubljana, SI-1000 Ljubljana, Slovenia*
[2]*Laboratorium für Festkörperphysik ETH Zurich, CH-8093 Zurich, Switzerland*
[3]*School of Physics, Trinity College Dublin, University of Dublin, Dublin 2, Ireland*
(Received 9 January 2007; revised manuscript received 15 June 2007; published 8 August 2007)

Optical reflectivity and absorbance measurements of oriented $Mo_6S_3I_6$ nanowire thin films and dispersions in different solvents are presented extending from the far infrared to the ultraviolet. In spite of the highly one-dimensional character of the nanowire material and narrow electronic valence and conduction subbands, as predicted by the density-functional theory calculations, sharp Van Hove features in the optical absorption spectra are not observed, partly because of the large density of interpenetrating electron subbands and partly due to damping and disorder. The optically measured electrical conductivity extrapolated to zero frequency $\sigma_1(\omega \rightarrow 0)$ and the calculated conductivity are significantly higher than the typical dc value from resistance measurements, indicating that disorder limits electron transport, a feature characteristic of strongly one-dimensional systems.

DOI: 10.1103/PhysRevB.76.075106 PACS number(s): 78.67.−n, 78.40.−q, 78.67.Ch

## I. INTRODUCTION

The optical properties of one-dimensional systems have received significant attention recently because of the inherent peculiarities in their electronic structure. Peaks in the density of states (Van Hove singularities) may lead to observation of sharp features in the optical spectra. A good example are single-walled carbon nanotubes[1,2] where peaks are observed in the absorption spectra corresponding to transitions between peaks in the density of states in good agreement with theoretical calculations. In the midinfrared, one-dimensional metallic systems may be expected to show Luttinger liquid-like power-law behavior of the optical conductivity.[3]

Molybdenum-based nanowires and nanotubes are examples of *inorganic* compounds for which strong one-dimensional effects were reported.[4–9] Among them, $Mo_6S_3I_6$ is of particular relevance for research and applications.[10,11] It synthesizes in bundles, 200–1000 nm in diameter, of identical molecular chains (wires).[12] The atomic structure of $Mo_6S_3I_6$ is shown in Fig. 1.[12,13] It is now confirmed that the molecules build one-dimensional chains of $Mo_6$ octahedra, each octahedron dressed with six anions and separated from neighboring octahedron by three bridging anions. In Fig. 1, the molecule with S atoms in the bridging planes and I atoms dressing the Mo octahedra is shown. The arrangement of individual molecular chains into bundles or into a crystal is less understood. Whereas the early x-ray diffraction data indicated a stacking in accordance with the $P6_3$ space group,[12] the most recent electron microscopy investigations suggest a much less symmetric $P\bar{1}$ space group.[13] In any case, it is clear from these studies that the attractive force, responsible for the bonding of individual molecular chains into bundles or crystals, is of dispersive, van der Waals type and thus weak.[12,13] These weak intermolecular forces are also responsible for the strongly one-dimensional electronic properties. Using a variety of solvents, the bundles can be dispersed into single molecular wires and as such have numerous possible applications in nanotechnology.[14] Mechanical,[15] tribological,[16] and electron transport measurements[17,18] confirm the strong one-dimensional (1D) character of these materials, suggesting that the interactions between molecular nanowires in $Mo_6S_3I_6$ bundles is even smaller than between the individual carbon nanotubes within bundles. dc electrical conductivity have shown strong 1D character, but the values of $\sigma_{dc}$ along the nanowires are still lower than the optical conductivity $\sigma_1(\omega \rightarrow 0)$ reported in this paper. This is thought to be a result of disorder in combination with the strongly one-dimensional character of the material. Evidence for the Tomonaga-Luttinger liquid behavior was observed in the temperature dependence of dc conductivity and current-voltage characteristics of $Li_2Mo_6Se_6$ nanowires,[19] and similar behavior is expected in $Mo_6S_3I_6$ based on their highly one-dimensional nature.

The present study reports on the optical measurements on freestanding films and oriented thin films on quartz substrates and in solution with the aim of elucidating the electronic structure and properties of these interesting new nanomaterials. As an aid to better understanding of the optical properties, we also performed the density-functional theory (DFT) simulations of the structures and optical properties.

## II. EXPERIMENTAL DETAILS

The $Mo_6S_3I_6$ samples were synthesized in a single step procedure as previously reported[11] (supplied by the company Mo6). The material was washed in isopropanol (IPA) to remove the unreacted iodine and possible impurity phases such as $Mo_6S_6I_2$ which quickly sedimented out. The resulting dispersion is decanted and passed through a quantitative membrane filter, which separates the bundles of $Mo_6S_3I_6$ nanowires from the solvent. Thin films were obtained by removal of the nanowires (NWs) from the membrane.

Oriented thin film samples were prepared on a quartz substrate by rubbing the NW material on the surface between two quartz plates. Scanning electron microscopy (SEM) and atomic force microscopy (AFM) images of the resulting films are shown in Figs. 2(a) and 2(b), respectively. The

 

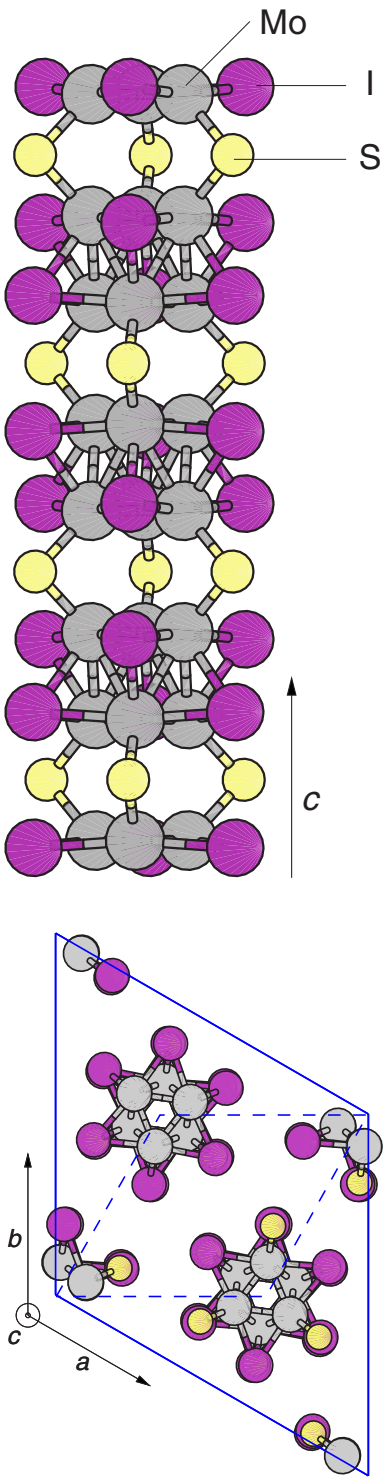


FIG. 1. (Color online) The atomic structure of $Mo_6S_3I_6$ nanowires. (a) Side view of an individual $Mo_6S_3I_6$ molecular chain with S atoms in the bridging positions and (b) projection along the crystalline $c$ axis. Early x-ray diffraction experiments indicated chain ordering according to the hexagonal $P6_3$ space group (Ref. 12) (the unit cell shown with solid lines), whereas the most recent electron microscopy experiments suggest the $P\bar{1}$ space group (Ref. 13) (dashed lines). The essential difference between the two space groups is the stacking, i.e., mutual displacements of individual molecular chains along the $c$ axis.

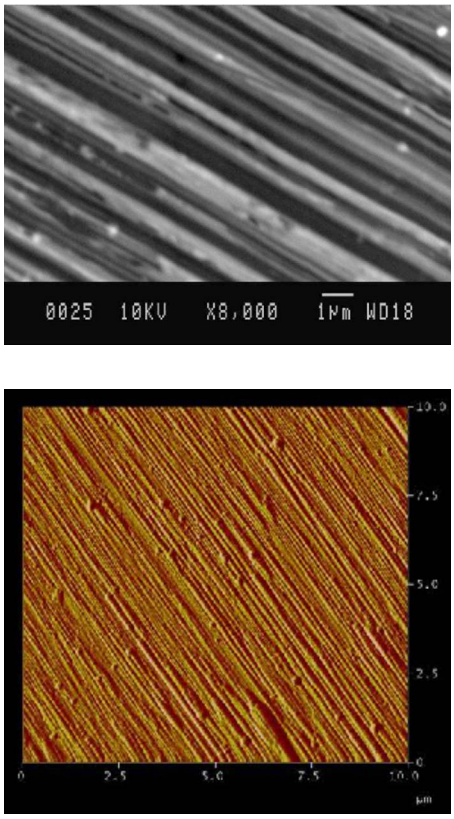


FIG. 2. (Color online) (a) A SEM image of the oriented $Mo_6S_3I_6$ film on quartz and (b) an AFM image of the oriented $Mo_6S_3I_6$ film on quartz. The image size is $10\times10$ $\mu m^2$. The surface roughness is approximately 8 nm, and the average film thickness is approximately 50 nm.

surface roughness of the NW film appears on the order of 8 nm. The degree of orientation appears to be very high, with nanowires running parallel to the rubbing direction, as confirmed in the optical spectra.

For the visible absorbance spectra in solution, 1 mg/ml solution was used. Sonication was performed for 30 min in a mild ultrasonic bath. When a majority of the sample had sedimented out of the solution (after ~1 h), the absorbance spectra were acquired. Subsequent sampling was also taken at regular time intervals to monitor further sedimentation or any other changes. The measurements were taken in a quartz spectroscopic cell and the solvent spectrum was subtracted each time. All the data presented were taken after one week of sedimentation. For the midinfrared measurements in solution, a 1 mg/ml dispersion of the $Mo_6S_3I_6$ material in $N,N$-dimethylformamide (DMF) was prepared. As this material is known to consist of a number of distinct phases, a solution based separation procedure was carried out. $Mo_6S_3I_6$ powder was dispersed in DMF by sonication and was allowed to sediment for 70 h before being decanted. The dispersion was then sonicated again and allowed to sediment for 600 h before being decanted for a second time. The remaining dispersion was dried in a vacuum oven with the two sediments and these three dried powders were weighted. Initially, 24.7 mg of washed $Mo_6S_3I_6$ material was dispersed in DMF. The masses of sediment 1, sediment 2, and the solute

recovered were 19.7 mg (~87%), 1.5 mg (~7%), and 1.4 mg (~6%), respectively, with 2.1 mg unrecoverable. The first sediment collect is known to consist of impurity material, while the second sediment consists of large bundles of nanowires. The dispersed phase consists of small bundles of $Mo_6S_3I_6$.[20] Therefore, after 600 h 6% of the $Mo_6S_3I_6$ was still dispersed in DMF, at a concentration of approximately 0.06 g/l. It is not clear whether this represents a solubility limit or perhaps the fact that the fraction of dispersible material in the washed powder was low. Nevertheless, it shows that it is possible to produce stable dispersions of $Mo_6S_3I_6$ with concentrations as high as 0.06 g/l. This compares reasonably well with achieved concentrations of 0.34 g/l for $Mo_6S_{4.5}I_{4.5}$ in isopropanol[21] or indeed of 0.02 g/l for single-walled nanotubes in 1-methyl-2-pyrolidinone.[22]

The IR absorbance spectra were acquired on Bomem 140 and 106 spectrometers, and an HP 8453 was used in the UV and visible regions. The reflectivity measurements were performed with a Bruker 113 Fourier transform infrared in air and corrected for scattering by evaporation of a gold film.

## III. DENSITY-FUNCTIONAL THEORY SIMULATIONS

For a better understanding of the optical and charge-carrier transport properties, we also performed DFT simulations using the WIEN2K code.[23] The chain ordering according to the $R\bar{3}c$, $R\bar{3}$, $P\bar{1}$, and $R3$ space groups were simulated.

The space groups $R\bar{3}c$, $R\bar{3}$, and $P\bar{1}$ describe almost identical intrachain ordering with three S atoms in the bridging planes (denoted as 3S); they differ from one another in the chain stacking, i.e., in the mutual displacements of individual molecular chains along the hexagonal $c$ axis. In the $P\bar{1}$ space group, the six neighboring chains are shifted along the $c$ axis by $\pm c/6$, $\pm c/3$, and $\pm c/2$; in the $R\bar{3}c$ and $R\bar{3}$ space groups, the displacements are $\pm c/3$, so that there are only three different chain displacements, whereas in the $P6_3$ space group (not simulated), two chains have arbitrary displacements. The essential difference between the $R3$ and the other three space groups is the exchange of S and I atoms: in $R3$, the S atoms are on the dressing positions and the I atoms in the bridging planes (denoted as 3I). All the simulated *primitive* cells contain 2 f.u. (30 atoms). First, the atomic coordinates and the lattice constants were optimized; for simulation details, see Ref. 24. In this stage, the energy was calculated on a tetrahedral mesh of 44 $k$ points in the irreducible part of the Brillouin zone. The energies were all within ±0.3 eV/f.u., the structure with the $P\bar{1}$ space group having the highest energy and the $R3$ structure having the lowest energy. In the following, we will concentrate on the structures belonging to the $R3$ and $R\bar{3}c$ spaceg roups. The band structure is sensitive not only to the chain stoichiometry but also to the isomerism and longitudinal strain.[12,24] The $R3$ and $R\bar{3}c$ isomers, thus, have different densities of states and Van Hove singularities, which reflect also in different optical properties. This property can be exploited for optical characterization of nanowires. However, typically, the accuracy of the calculation presented here is comparable to the predicted differences in the electronic properties, so we rely on the present calculation to give us the salient features of the optical spectra, and not necessarily the detailed spectral features.

The dielectric response of nanowires implies excitations of electrons across the Fermi energy, whereas the DFT is a ground-state method. Often, the independent-particle approximation is used to investigate the charge-carrier excitations. This random-phase approximation (RPA) usually works well for three-dimensional metals, where the interaction between the charges is strongly screened by the conducting electrons and therefore the charges can be regarded as approximately independent. For semiconductors or insulators and for low-dimensional systems, this is no longer true and different approximations are becoming available which go beyond the RPA and which include the electron-hole or quasiparticle correlations.[25–27] In this paper, we still make use of the RPA, which is the only available approach in the WIEN2K code for the time being.[28] Due to the neglection of the electron-hole correlations and, in particular, of the bound exciton states, the electron band gaps in semiconductors and insulators are underestimated and this is reflected in the optical spectra.

In the next sections, we will compare the experimental optical properties with the calculated results. A mesh of 288 $k$ points and an energy window $E_F \pm 45$ eV were used ($E_F$ is the Fermi energy) in the simulations. The large energy window is needed to fulfill the sum rules and the Kramers-Kronig relations which are used to obtain the optical properties from the dielectric functions. We assume that the longitudinal and transverse intraband charge-carrier scattering, responsible for the low-frequency and static conductivities, are described by the damping $\Gamma_\parallel = \Gamma_\perp = 0.5$ eV. With such values, the charge carriers are localized along individual molecular chains with the longitudinal charge-carrier mean-free path of the order of 1–2 nm, close to the Ioffe-Regel limit.

## IV. OPTICAL REFLECTIVITY

The optical reflectivity of freestanding nonoriented thin films was measured over a broad spectral range extending from the far infrared to the visible and as a function of temperature by employing a variety of spectrometers.[3] All optical functions, such as the real part of the optical conductivity $\sigma_1$, the refraction index $n$, the absorption coefficient $k$, and the real and imaginary parts of the dielectric function $\epsilon$, were then obtained by applying the Kramers-Kronig transformations.[29,30] Figure 3(a) displays the measured reflectivity at 300 K for two samples. Sample 1 was annealed at 200 °C in vacuum, while sample 2 was not. The annealing process clearly enhances the overall $R(\omega)$, leaving, however, its shape and trend unchanged. We have collected data on several spots of the sample surface. While slightly different spectra were obtained from spot to spot, the main features were always identified and Fig. 3(a) is representative of the general trend of our data. The freestanding film was not totally flat and the surface corrugation and waviness induced a lot of scattering (particularly at low energies). The reflectivity was then corrected by the measurement of the sample

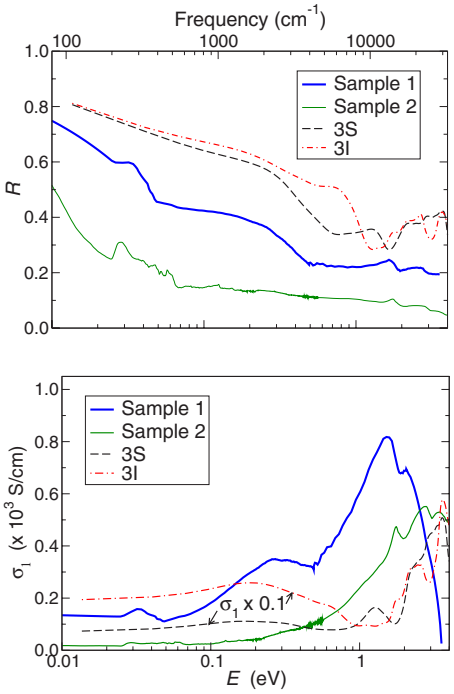


FIG. 3. (Color online) (Top) The reflectivities $R(\omega)$ of annealed (sample 1) and unannealed (sample 2) samples and the calculated $R(\omega)$ for two isomers (3S and 3I) and random polarizations. (Bottom) The optical conductivity $\sigma_1(\omega)$ of the two samples, derived from $R(\omega)$, and the calculated $\sigma_1(\omega)$, multiplied by 0.1. In this and the following figures, the isomer 3S has S atoms in the bridging positions, whereas in the case labeled 3I, the bridging atoms are I, and the S atoms occupy the dressing positions. In the simulations, the intraband transitions (Drude peak) are damped with $\Gamma=0.5$ eV and the interband transitions with $\Gamma=0.1$ eV.

coated with a thin gold layer. This actually acts as the reference measurement, taking also into account the surface irregularities. We did not find any temperature dependence in the measured spectral range. While the data were collected down to 30 cm$^{-1}$, below 70 cm$^{-1}$ they were no longer reproducible. At such long wavelengths, the data are not anymore reliable since the wavelength was comparable to the sample thickness. The high frequency reflectivity was extrapolated with a broad harmonic oscillator centered at $4\times10^4$ cm$^{-1}$. At low frequency, it is possible to extrapolate the reflectivity in a metalliclike fashion by using a Hagen-Rubens (HR) extrapolation with a $\sigma_{dc}$ value of about 170 S/cm for sample 2 and 45 S/cm for sample 1.

Figure 3(b) shows the real part $\sigma_1$ of the optical conductivity of the two samples. The overall trend of the optical conductivity is very much indicative of a semimetal. Besides a few absorptions in the far infrared, which we ascribe to phonon modes, there is the onset of a rather strong absorption around 2000 cm$^{-1}$, merging in the peak at about $10^4$ cm$^{-1}$ (sample 1), which could be ascribed to a kind of pseudogap. It is, however, interesting to observe that a broad metalliclike background (i.e., Drude weight) persists in the optical conductivity. It is associated with the plasma-edgelike feature, which can be recognized in the optical reflectivity [Fig. 3(a)] below 4000 cm$^{-1}$. The HR extrapolation of

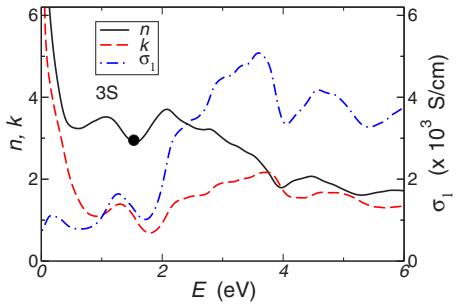


FIG. 4. (Color online) The calculated complex refractive index $(n,k)$ and conductivity $\sigma_1$ for the 3S structure and for random polarizations. The solid circle is an ellipsometrically measured value of the refractive index $n$ at 1.53 eV (Ref. 31).

$R(\omega)$ suggests indeed the presence of a weak metallic component in the optical spectra. We shall stress, nevertheless, that the optical conductivity is very much independent of the low-frequency extrapolation. This is because the reflectivity has an overall "overdampedlike" behavior. Similar spectra were also obtained for amorphous and quasicrystalline materials,[32] as well as for carbon nanotube films.[1] Above ~2 eV, $\sigma_1$, extracted from the reflectivity data, is suppressed because of the strong surface light scattering. Since the nanowire samples in the reflectivity experiments are not oriented, we cannot perform polarization dependent optical investigations. For this reason, we must assume that our data suffer from the projections of different directions. This also prevents the search for possible characteristic power-law behavior in $\sigma_1(\omega)$, which might be indicative for a Tomonaga-Luttinger liquid state.[3]

The calculated reflectivity, also shown in Fig. 3(a), is up to ~0.5 eV dominated by the semimetallic Drude conductivity and is relatively featureless. The fact that the calculated $R(\omega)$ exceeds the experimental data is indicative that sample 1 is still strongly disordered. The calculated complex refractive index $(n,k)$ and $\sigma_1$, obtained via the Kramers-Kronig transformation of $\mathrm{Im}(\varepsilon)$ together with the Drude peak and averaged over all directions, are displayed in Fig. 4. It is worth noting that the ellipsometrically measured value[31] of the refractive index $n=2.95$ at 1.53 eV agrees remarkably well with the calculation. Nevertheless, above 2 eV, the strong surface light scattering makes a direct comparison between experiment and theory rather difficult. In this respect, absorbance measurements, to be reported and discussed below, give an enhanced sensitivity.

## V. ABSORBANCE IN ORIENTED FILMS

In Fig. 5, we present the experimental absorption spectra for $E\|c$ and $E\perp c$ polarizations, where $c$ refers to the hexagonal crystallographic axis. We clearly observe distinct spectra for the two polarizations. $E\perp c$ polarization is much smoother and shows no evidence of any of the features appearing in $E\|c$ polarization, indicating a high degree of alignment.

The calculated spectra for two isomers of $Mo_6S_3I_6$ (also shown in Fig. 5) are, like the experimental ones, rather fea-

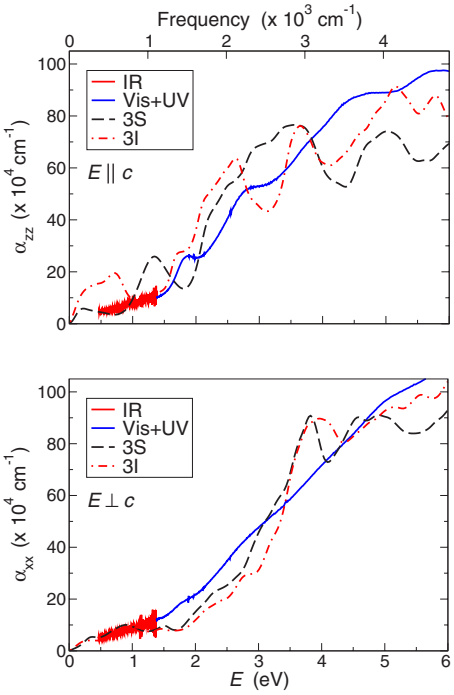


FIG. 5. (Color online) Optical absorbance in oriented thin films. Top panel refers to the polarization parallel to the long molecular axis and bottom panel to the perpendicular polarization. Solid lines are from the experiment (arbitrary scale), and the other lines are calculated in the RPA.

tureless below ~4 eV for the $E \perp c$ polarization. Above ~4 eV, the optical transitions *between the chains*, which are more structured, start to contribute. In the case of the $E \| c$ spectra, we associate the 1.4 eV peak of the 3S isomer with the S $3p \rightarrow$ Mo $4d$ excitations and the 3.5 eV peak mainly to Mo $4d \rightarrow$ Mo $4d$ transitions with Mo atoms on different sites. The main contributions to the peak at ~2.6 eV of the 3I isomer come from I $5p \rightarrow$ Mo $4d$ and S $3p \rightarrow$ Mo $4d$ excitations. By comparing the calculated and experimental absorption spectra, we see that both show the same general trend of increasing $\alpha$ with frequency and that the calculated spectra are more structured than the experimental ones. The discrepancy between the experiment and theory is ascribed to the RPA, which neglects electron-hole correlations. It is known from other systems, such as $MoS_2$, that the S $3p \rightarrow$ Mo $4d$ charge transfer peak is around 1.8 eV.[33] In $Mo_6S_3I_6$ (Fig. 5), this transition appears clearly at 1.75 eV for $E \| c$. This suggests that the energy of the calculated 1.4 eV peak is underestimated by ~25%.

## VI. ABSORBANCE IN SOLUTION

To determine the possible solvatochromic effects of $Mo_6S_3I_6$ nanowires in solution, we compare data on solid unoriented films with absorbance in different popular solvents.[34] The solutions which were prepared as discussed above were stable over long periods of time. Aggregation could be seen to cause a slight linear shift of the whole spectra, but we could not detect a decrease of the peak amplitudes. Further sonification of the prepared solution for a few hours also had no effect, indicating that the solution is stable. The absorbance spectra for $Mo_6S_3I_6$ in water, acetone, isopropanol, and ethanol are shown in Fig. 6. For comparison, the spectrum for $Mo_6S_{4.5}I_{4.5}$ is also shown. One feature that stands out is the peak near 5.5 eV which is present strongly in water and weakly at 5.7 eV in ethanol. Other peaks do not appear to show any differences between different solvents.

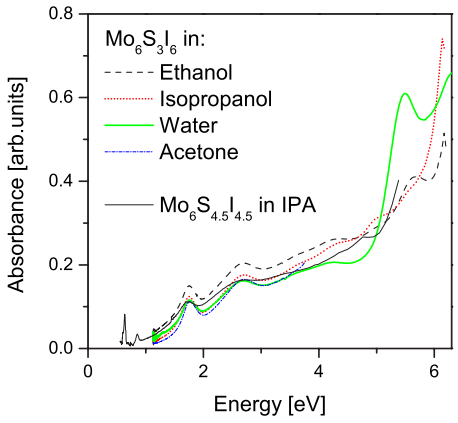


FIG. 6. (Color online) The absorption spectra of $Mo_6S_3I_6$ nanowires in different solvents. $Mo_6S_{4.5}I_{4.5}$ in IPA is shown for comparison from Ref. 34.

In the ultraviolet-visible region, there are no major differences between the sediments and solute described in Sec. II. The optical transitions in this energy range are thus unaffected by the interchain separations or stacking and are therefore associated with the intrachain electronic transitions. In the near IR region (~0.6–0.8 eV), this is no longer true. To measure the near infrared spectra, each of the three recovered powders, sediment 1, sediment 2, and the solute, was redispersed in IPA. For comparison purposes, the $Mo_6S_3I_6$ soot was also dispersed in IPA. The spectra are shown in greater detail in Fig. 7. In the range from approximately 0.7 to 0.75 eV, noise is due to the subtraction of the IPA peaks from the individual spectra, so no peaks are visible. In sediment 2 and in the solute, a distinct peak is observed at 0.64 eV with a smaller shoulder at 0.66 eV. This demonstrates the similarity between these two phases, which both contain $Mo_6S_3I_6$ nanowires, as observed in the transmission and scanning electron microscopy images. Such a feature has also been observed for $Mo_6S_{4.5}I_{4.5}$ nanowires.[34] The position of this peak agrees reasonably well with predictions for the $Mo_6S_3I_6$ band gap,[12] suggesting that it may represent a transition involving the Van Hove singularity associated with the band edge. All these features are visible in the washed $Mo_6S_3I_6$ sample, which should be a combination of these three phases, as was expected, although the peak at 0.64 eV is quite weak due to the high intensity of the near infrared peaks in sediment 1. At 0.64 eV in the sediment 1 spectrum, all that is visible is the noise due to the IPA peaks present in this region.

A comparison between the ethanol solution and the thin solid film is shown in Fig. 8. We observe a redshift of the peaks in solution by ~−0.1−1.74, 2.7, 4.32, and 5.67 eV

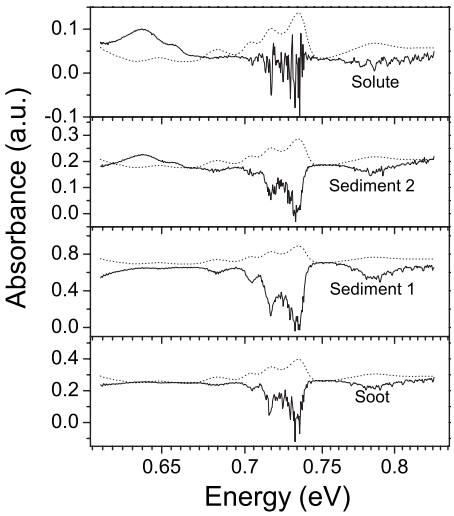


FIG. 7. The absorption spectra in the near infrared region of different $Mo_6S_3I_6$ sediments redispersed in IPA (solid lines). Pure IPA is shown for comparison (dotted line).

compared to the thin film. The redshift does not appear to depend strongly on the degree of debundling, indicating that it is most likely caused by the dielectric constant of the solvent rather than any possible change in the spectrum due to interwire interactions.

## VII. DISCUSSION

The main issue of the paper is the experimental determination of optical properties of $Mo_6S_3I_6$ nanowires, as observed in the reflectivity and absorption measurements in solid oriented films and in solutions. An unusual feature of the optical spectra is that no sharp features are visible, in spite of the strong one-dimensional character of the electronic bands and relatively sharp features in the density of states.[24] One reason is that there is a multitude of narrow subbands which belong to Mo $d$ derived orbitals and which lie in the region ±2 eV from $E_F$ (note that transitions between single-ion $d$ levels are parity forbidden). The first observed clear peak at 1.8 eV most likely involves transitions

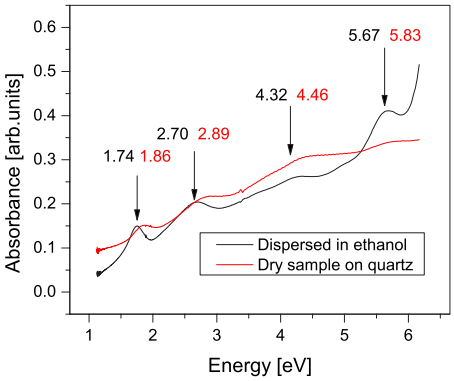


FIG. 8. (Color online) The absorption spectra of $Mo_6S_3I_6$ nanowires in ethanol and measured on a thin film.

between occupied S $p$ states just below the Fermi energy and unoccupied Mo $d$ states on the same chain. Since all the spectra presented here were taken at room temperature, the transitions are also broadened by phonon-assisted processes. Moreover, mechanical deformation caused by the processing of thin films is also expected to cause broadening. The $Mo_6S_3I_6$ nanowires in bulk form are very malleable, which means that individual bundles and strands are easily deformed. This is expected to result in symmetry-breaking effects as well as broadening of electronic transitions due to structural deformations.

From the fact that the reflectance and whence optical conductivity are strongly sample dependent, the dc limits of the optical conductivity $[\sigma_1(\omega \rightarrow 0) \sim 45-170\ \mathrm{S/cm}]$ are much higher than the measured dc transport values ($\sigma_{dc} \sim 0.1\ \mathrm{S/cm}$), which is an indication that the dc transport is limited by imperfections, such as broken chains or stoichiometric disorder. With the charge-carrier mean-free path $\lambda_m = 1$ nm (i.e., unit cell size along the length), the calculated conductivity is on the order of $\sigma_1(\omega \rightarrow 0) \sim 800\ \mathrm{S/cm}$ (3S isomer), which is a factor of 5 larger than the measured value from reflectivity. Such a value of $\lambda_m$ is already close to the Ioffe-Regel limit. The discrepancy might be partially the consequence of the random-phase approximation in the optical calculations and partially due to abovementioned disorder and mechanical imperfections of the material, which lead to electron localization and reduced dc conductivity. It may be argued that thermal fluctuations in the strongly one-dimensional material may be the cause of the relatively low observed conductivity. Of course, such thermally induced fluctuations would also be present in $Li_2Mo_6Se_6$ nanowires. However, in this system, rather convincing evidence for the Tomonaga-Luttinger liquid behavior and ballistic conductance has been observed,[8] which would not have been observed if thermal fluctuations limited the conductivity. Thus, it appears that in $Mo_6S_{9-x}I_x$, built-in disorder limits the electron transport.

An important related issue from the material preparation point of view pertains to the determination of S and I site occupancy on the $Mo_6S_3I_6$ skeletal backbone. Determination of site occupancy on the "bridging" and "dressing" positions is crucially important for improved material preparation and achievement of higher conductivity and other functional properties which depend on stoichiometry and isomerism. Optical spectra on oriented samples have been shown to be sensitive to intrachain structure, to distinguish between different isomers, much better than x-ray scattering, extended x-ray-absorption fine structure, or pair distribution function techniques, which can give very accurate atomic positions but not so much atomic occupancies. However, further work beyond RPA is needed to improve the accuracy of the calculated optoelectronic properties. The DFT simulations of $Mo_6S_3I_6$ ordered in four different space groups ($P\bar{1}$, $R\bar{3}c$, $R\bar{3}$, and $R3$) give very similar binding energies in all these cases. The final structure may, therefore, depend on the process of synthesis. Nevertheless, we can expect a certain degree of disorder in the occupation of anion sites (substitutional disorder) and, in particular, in the chain displacements along the $c$ axis. The latter disorder may be the reason for the low

symmetry space group reported in Ref. 13 also.

The calculated bulk dispersion of the electron bands is of the order of 0.5 eV in the longitudinal direction and 0.1 eV in the transverse plane. Small dispersion in the transverse plane is responsible—together with imperfections in the crystal structure—for the charge-carrier localization and consequently hopping transport in this plane and for the quasi-one-dimensional conductivity along the chain axis.

We conclude by noting that the low-frequency semimetallic conductivity in combination with very anisotropic dispersion characteristics in different polymers is expected to be very promising for microwave shielding applications. Improving synthesis to reduce disorder is expected to significantly increase the dc conductivity.

## ACKNOWLEDGMENTS

One of us (L.D.) wishes to thank J. Mueller for technical help. This work was supported in part by the Slovenian Research Agency under the Contract Nos. P1-0044 and P1-0040 and the EU DESYGN-IT project. The crystal structures were visualized by XCRYSDEN.[35]

[1] B. Ruzicka, L. Degiorgi, R. Gaal, L. Thien-Nga, R. Bacsa, J.-P. Salvetat, and L. Forró, Phys. Rev. B **61**, R2468 (2000).
[2] H. Kataura, Y. Kumazawa, Y. Maniwa, I. Umezu, S. Suzuki, Y. Ohtsuka, and Y. Achiba, Synth. Met. **103**, 2555 (1999).
[3] V. Vescoli, L. Degiorgi, W. Henderson, G. Grüner, K. P. Starkey, and L. K. Montgomery, Science **281**, 1181 (1998).
[4] M. Potel, R. Chevrel, M. Sergent, J. C. Armici, M. Decroux, and O. Fischer, J. Solid State Chem. **35**, 286 (1980).
[5] J. M. Tarascon, F. J. DiSalvo, and J. V. Warszczak, Solid State Commun. **52**, 227 (1984).
[6] J. M. Tarascon, G. W. Hull, and F. J. DiSalvo, Mater. Res. Bull. **19**, 915 (1984); J. M. Tarascon, J. Electrochem. Soc. **132**, 2089 (1985).
[7] R. Brusetti, P. Monceau, M. Potel, P. Gougeon, and M. Sergent, Solid State Commun. **66**, 181 (1988).
[8] L. Venkataraman and C. M. Lieber, Phys. Rev. Lett. **83**, 5334 (1999).
[9] F. J. Ribeiro, D. J. Roundy, and M. L. Cohen, Phys. Rev. B **65**, 153401 (2002).
[10] T. Yang, S. Okano, S. Berber, and D. Tománek, Phys. Rev. Lett. **96**, 125502 (2006).
[11] D. Vrbanic, M. Remškar, A. Jesih, A. Mrzel, P. Umek, M. Ponikvar, B. Jančar, A. Meden, B. Novosel, S. Pejovnik, P. Venturini, J. N. Coleman, and D. Mihailovic, Nanotechnology **15**, 635 (2004).
[12] A. Meden, A. Kodre, J. Padeznik Gomilsek, I. Arcon, I. Vilfan, D. Vrbanic, A. Mrzel, and D. Mihailovic, Nanotechnology **16**, 1578 (2005).
[13] V. Nicolosi, P. D. Nellist, S. Sanvito, E. C. Cosgriff, S. Krishnamurthy, W. J. Blau, M. L. H. Green, J. Sloan, D. Vengust, D. Dvorsek, D. Mihailovic, G. Compagnini, V. Stolojan, J. D. Carey, and J. N. Coleman, Adv. Mater. (Weinheim, Ger.) **19**, 543 (2007).
[14] V. Nicolosi, D. Vengust, D. Mihailovic, W. J. Blau, and J. N. Coleman, Chem. Phys. Lett. **425**, 89 (2006).
[15] A. Kis, D. Mihailovic, M. Remškar, A. Mrzel, A. Jesih, I. Piwonski, A. J. Kulik, W. Benoît, and L. Forró, Adv. Mater. (Weinheim, Ger.) **15**, 733 (2003).
[16] L. Joly-Pottuz, F. Dassenoy, M. Belin, B. Vacher, J. M. Martin, and N. Fleischer, Tribol. Lett. **18**, 477 (2005).
[17] B. Bercic, U. Pirnat, P. Kusar, D. Dvoršek, and D. Mihailovic, Appl. Phys. Lett. **88**, 173103 (2006).
[18] M. Uplaznik, B. Berčič, J. Strle, M. Ploscaru, D. Dvoršek, P. Kušar, M. Devetak, D. Vengust, B. Podobnik, and D. Mihailovic, Nanotechnology **17**, 5142 (2006).
[19] L. Venkataraman, Y. S. Hong, and P. Kim, Phys. Rev. Lett. **96**, 076601 (2006).
[20] V. Nicolosi, D. N. McCarthy, D. Vengust, D. Mihailovic, W. J. Blau, and J. N. Coleman, Eur. Phys. J.: Appl. Phys. **37**, 149 (2007).
[21] V. Nicolosi, D. Vrbanic, A. Mrzel, J. McCauley, S. O'Flaherty, D. Mihailovic, W. J. Blau, and J. N. Coleman, Chem. Phys. Lett. **401**, 13 (2005).
[22] S. Giordani, S. D. Bergin, V. Nicolosi, S. Lebedkin, M. M. Kappes, W. J. Blau, and J. N. Coleman, J. Phys. Chem. B **110**, 15708 (2006).
[23] P. Blaha, K. Schwarz, G. K. H. Madsen, D. Kvasnicka, and J. Luitz, WIEN2K, a full potential LAPW package, TU Vienna, 2001.
[24] I. Vilfan and D. Mihailovic, Phys. Rev. B **74**, 235411 (2006).
[25] E. Runge and E. K. U. Gross, Phys. Rev. Lett. **52**, 997 (1984).
[26] M. Rohlfing and S. G. Louie, Phys. Rev. B **62**, 4927 (2000).
[27] C. D. Spataru, S. Ismail-Beigi, L. X. Benedict, and S. G. Louie, Phys. Rev. Lett. **92**, 077402 (2004); Appl. Phys. A: Mater. Sci. Process. **78**, 1129 (2004).
[28] J. O. Sofo and C. Ambrosch-Draxl, Comput. Phys. Commun. **175**, 1 (2006).
[29] F. Wooten, *Optical Properties of Solids* (Academic, New York, 1972).
[30] M. Dressel and G. Grüner, *Electrodynamics of Solids* (Cambridge University Press, Cambridge, 2002).
[31] P. Kusar and D. Mihailovic, J. Appl. Phys. **102**, 013510 (2007).
[32] A. D. Bianchi, F. Bommeli, M. A. Chernikov, U. Gubler, L. Degiorgi, and H. R. Ott, Phys. Rev. B **55**, 5730 (1997).
[33] J. A. Wilson and A. D. Yoffe, Adv. Phys. **18**, 193 (1969).
[34] V. Nicolosi, D. Vrbanic, A. Mrzel, J. McCauley, S. O'Flaherty, C. McGuinness, G. Compagnini, D. Mihailovic, W. J. Blau, and J. N. Coleman, J. Phys. Chem. B **109**, 7124 (2005).
[35] A. Kokalj, J. Mol. Graphics Modell. **17**, 176 (1999). Code available from http://www.xcrysden.org/